Rattle-Structured Nanoprobe

Deutsche Ausgabe: DOI: 10.1002/ange.201501468
Internationale Ausgabe: DOI: 10.1002/anie.201501468

Multifunctional Nano-Bioprobes Based on Rattle-Structured Upconverting Luminescent Nanoparticles**

*Shan Lu, Datao Tu, Ping Hu, Jin Xu, Renfu Li, Meng Wang, Zhuo Chen, Mingdong Huang, and Xueyuan Chen**

Abstract: *Lanthanide-doped upconversion nanoparticles (UCNPs) have shown great promise in versatile bioapplications. For the first time, organosilica-shelled β-$NaLuF_4$:Gd/Yb/Er nanoprobes with a rattle structure have been designed for dual-modal imaging and photodynamic therapy (PDT). Benefiting from the unique rattle structure and aromatic framework, these nanoprobes are endowed with a high loading capacity and the disaggregation effect of photosensitizers. After loading of β-carboxyphthalocyanine zinc or rose Bengal into the nanoprobes, we achieved higher energy transfer efficiency from UCNPs to photosensitizers as compared to those with conventional core–shell structure or with pure-silica shell, which facilitates a large production of singlet oxygen and thus an enhanced PDT efficacy. We demonstrated the use of these nanoprobes in proof-of-concept X-ray computed tomography (CT) and UC imaging, thus revealing the great potential of this multifunctional material as an excellent nanoplatform for cancer theranostics.*

With the development of biomedicine, functional combination of diagnosis and therapy (the so-called "theranostics") becomes a new trend. The detected lesions or tumors are expected to receive treatment concurrently with reducing the risk of repeated dosing or surgery. To achieve concise and effective theranostics, a nanoplatform integrated with functions of target specificity, multimodal imaging, and therapeutic properties is required. Lanthanide-doped upconversion nanoparticles (UCNPs) that can convert the near-infrared (NIR) light into visible light offer excellent prospects in developing new non-invasive strategies for theranostics. UCNPs as luminescent nanoprobes for bioimaging exhibit superior features, such as low toxicity, no photobleaching, background-free fluorescence, and a remarkable light penetration depth in biological specimens.[1] Moreover, UCNPs can be applied in a photodynamic therapy (PDT) wherein photosensitizers are activated by UCNPs under NIR excitation to generate cytotoxic singlet oxygen ($^1O_2$) and thus enable the treatment of large or internal tumors.[2]

Recently, various UCNP-silica nanocomposites have been constructed for bioimaging and NIR-triggered PDT both in vitro and in vivo.[2a,3] The bottleneck for the practical application of these nanocomposites lies in their low PDT efficacy. As the efficacy of PDT is dependent on the efficiency of energy transfer from UCNPs to the photosensitizers, sufficient photosensitizers loaded adjacent to UCNPs are essential. However, most of previous systems suffer from low loading capacity of photosensitizers; for instance, only 0.25 wt % for merocyanine-540 and 0.34 wt % for zinc phthalocyanine were reported to be adsorbed in a mesoporous silica coated UCNP.[2a] It is not recommended to increase the loading simply by a thicker shell of silica, because a distance that is too long between photosensitizers and UCNPs may result in inefficient energy transfer. To overcome these concerns, we propose a strategy to fabricate a novel rattle structure with a cavity between UCNP and porous silica shell. Rattle structure is a research hotspot in drug delivery, catalysis, and energy storage owing to its high payload for guest molecules.[4] The interior cavity can accommodate photosensitizers and also shorten their distance to UCNPs. Additionally, most of photosensitizers have structures with a planar conjugated aromatic ring and tend to aggregate in aqueous environment, which leads to self-quenching and hampers the generation of $^1O_2$.[3c] In this regard, benzene-bridged organosilica can be incorporated in the system to tailor the interaction between photosensitizers and silica shell. Through hydrophobic interaction and π–π overlapping aromatic framework is anticipated to enhance the adsorption of photosensitizers and prevent them from aggregation. To the best of our knowledge, utilization of benzene-bridged organosilica to attain the disaggregation of photosensitizers has not been reported before.

Herein, a multifunctional rattle-structured upconversion (UC) nano-bioprobe is judiciously designed with the core of β-$NaLuF_4$:Gd/Yb/Er and the shell of benzene-bridged organosilica (Figure 1). β-$NaLuF_4$, which is one of the most efficient UC hosts and an X-ray computed tomography (CT) contrast agent, is aimed to achieve UC and CT dual-modal imaging. Rattle structure and aromatic bridging groups are

[*] Dr. S. Lu, Dr. D. T. Tu, J. Xu, R. F. Li, Dr. M. Wang, Prof. Dr. X. Y. Chen
Key Laboratory of Optoelectronic Materials Chemistry and Physics
Fujian Institute of Research on the Structure of Matter
Chinese Academy of Sciences, Fuzhou, Fujian 350002 (China)
E-mail: xchen@fjirsm.ac.cn
P. Hu, Dr. Z. Chen, Prof. M. Huang
State Key Laboratory of Structural Chemistry
Danish–Chinese Centre for Proteases and Cancer
Fujian Institute of Research on the Structure of Matter
Chinese Academy of Sciences, Fuzhou, Fujian 350002 (China)

[**] We thank Prof. Fuyou Li and Dr. Wei Feng for the computed tomography experiments and cellular imaging. This work is supported by the 973 program of MOST (No. 2014CB845605), Special Project of National Major Scientific Equipment Development of China (No. 2012YQ120060), the NSFC (Nos. 21201163, U1305244, and 21325104), the CAS/SAFEA International Partnership Program for Creative Research Teams, Strategic Priority Research Program of the CAS (No. XDA09030307), and NSF of Fujian Province (No. 2013J05038).

Supporting information for this article is available on the WWW under http://dx.doi.org/10.1002/anie.201501468.

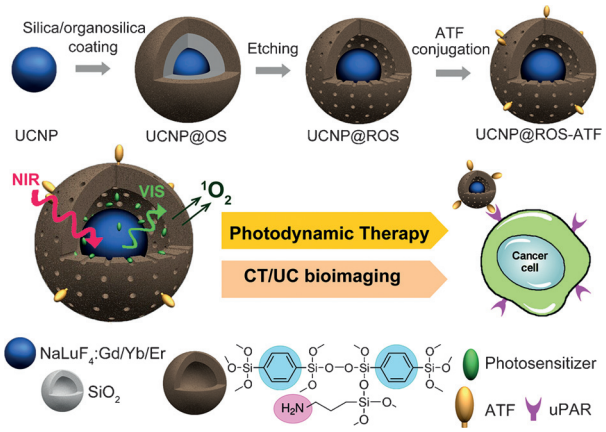

Figure 1. Illustration of multifunctional nano-bioprobes based on rattle-structured organosilica-shelled UCNPs.

introduced to increase the storage of photosensitizers, avoid their aggregation, and promote energy transfer. The amino terminal fragment (ATF) of urokinase plasminogen activator (uPA), which has a high affinity of uPA receptor (uPAR),[5] is further conjugated on the shell to render nano-bioprobes tumor-targeting. Such a nanoplatform designing offers a new route to load PDT drugs and should be highly promising as a nanocarrier for cancer theranostics.

Monodisperse oleate-capped β-$NaLuF_4$:Gd/Yb/Er nanoparticles (NPs) were prepared by a modified thermal decomposition followed by the seed-mediated growth.[6] Gd^{3+}-doping was introduced to help the formation of pure hexagonal-phase $NaLuF_4$:Gd/Yb/Er seeds. After growing

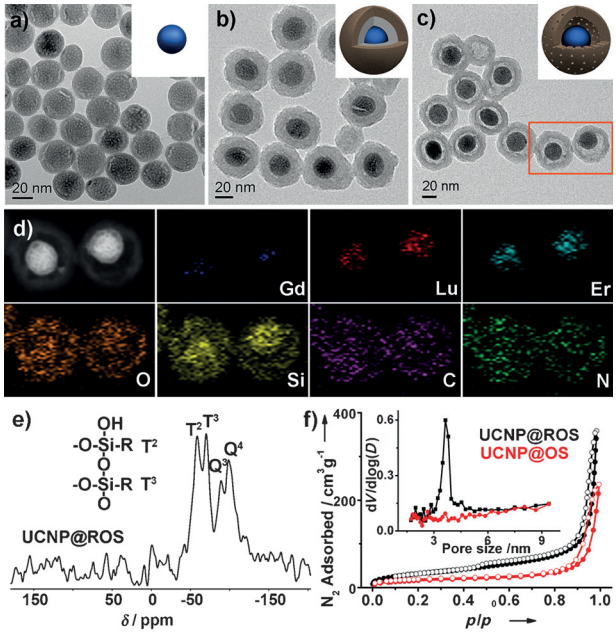

Figure 2. TEM images of a) β-$NaLuF_4$:Gd/Yb/Er (UCNP), b) UCNP@OS, and c) UCNP@ROS. d) STEM and corresponding elemental (Gd, Lu, Er, O, Si, C, N) mappings of UCNP@ROS. e) ^{29}Si CP/MAS NMR of UCNP@ROS. f) N_2 adsorption–desorption isotherms (● adsorbtion, ○ desorption) and pore size distribution of UCNP@OS and UCNP@ROS.

with $NaLuF_4$:Yb/Er layer, the resulting UCNPs possessed uniform spherical morphology with a diameter of about 27 nm, as shown in transmission electron microscope (TEM) image (Figure 2a). A powder X-ray diffraction (XRD) pattern (Supporting Information, Figure S1) confirms the hexagonal phase of the sample. Upon a 980 nm laser excitation at a power density of 130 $W\,cm^{-2}$, the absolute UC quantum yield (QY) of β-$NaLuF_4$:Gd/Yb/Er was determined to be 2.7%. Silica coating of UCNPs was conducted by a reverse microemulsion method. Tetraethylorthosilicate (TEOS) was added to form a thin pure-silica shell and the organosilica was then deposited as the outer shell through hydrolysis of 1,4-bis(triethoxysilyl)benzene (BTEB) and 3-aminopropyl triethoxysilane (APTES). The shell thickness of the organosilica-coated UCNPs (designated as UCNP@OS) is estimated to be about 10 nm by TEM (Figure 2b). Finally, UCNP@OS was directly converted into rattle structure by a method of "surface-protected etching" as previously reported.[4c] TEM image in Figure 2c shows the morphology of resulting rattles (designated as UCNP@ROS). The inner silica was etched, leaving an internal cavity between the UCNP core and the outer organosilica shell. Elemental mappings by scanning transmission electron microscopy (STEM) measurement clearly reveal that the Lu-containing UCNP is located within the organosilica shell and Gd^{3+} ions are doped only at the interior core of UCNP (Figure 2d). Moreover, phenylene and amine groups distribute homogeneously in the organosilica framework according to element mapping of C and N. The ^{29}Si cross-polarization magic-angle-spinning (CP-MAS) solid-state NMR spectrum in Figure 2e confirms the incorporation of organosilica. Along with Si environments of Q^4 at −110 ppm and Q^3 at −100 ppm ($Q^n = Si(OSi)_n(OH)_{4-n}$), UCNP@ROS displays two more resonance peaks at −80.5 ppm and at −68.4 ppm, which were assigned to the Si atoms of T^2 and T^3 units ($T^n = RSi(OSi)_n(OH)_{3-n}$), respectively.

Nano-rattles with a pure-silica shell (designated as UCNP@RS) were also prepared for comparison (Supporting Information, Figure S2a). The differences in surface properties between UCNP@ROS and UCNP@RS were characterized by FTIR spectroscopy and ζ-potential measurements (Supporting Information, Figures S3, S4). Generally, it takes more etching time to make internal cavity for an organosilica shell than a pure-silica shell owing to the higher hydrothermal stability of the former.[7] Specifically, etching in water at 95 °C for 6 h generated about 3 nm of cavity in UCNP@ROS while etching for 3 h was sufficient for the generation of the same-size cavity in UCNP@RS. N_2 adsorption–desorption analysis (Figure 2f; Supporting Information, Table S1) provides more information for the rattle structure. Through etching process, additional pores appeared with sizes distributed at 3.2–4.0 nm, and the surface area increased from 53 to 117 $m^2\,g^{-1}$ and the pore volume increased from 0.33 to 0.55 $cm^3\,g^{-1}$, indicating a higher capacity for UCNP@ROS. Furthermore, by changing the shell thickness and the etching time, the interior cavity can be tuned from less than 1 nm to about 5 nm (Supporting Information, Figure S2b,c). The synthetic conditions and textural parameters of all the nanocomposites with various structures and frameworks are summarized in

the Supporting Information, Table S1. Upon NIR excitation at 980 nm, UCNP@ROS exhibited characteristic sharp emission peaks, which are attributed to the $^2H_{11/2}\rightarrow{}^4I_{15/2}$ (521 nm), $^4S_{3/2}\rightarrow{}^4I_{15/2}$ (541 nm), and $^4F_{9/2}\rightarrow{}^4I_{15/2}$ (654 nm) transitions of Er^{3+} (Supporting Information, Figure S5).

Monosubstituted β-carboxyphthalocyanine zinc (ZnPc-COOH), the absorption band of which overlaps well with the red UC emission of Er^{3+} (Supporting Information, Figure S6), was chosen as a model photosensitizer to investigate the loading performance and the PDT efficacy of UCNP@ROS. The tiny pores at the organosilica shell and the interior cavity favor the accommodation of ZnPc-COOH, resulting in a loading amount as high as 7.7 wt% (Supporting Information, Table S2). Furthermore, the phenylene and amine groups in the shell play an importance role in adsorption of ZnPc-COOH via hydrophobic interactions, π–π overlapping, and electrostatic attractions. By contrast, only 2.7 wt% of ZnPc-COOH was loaded in UCNP@OS with a normal core–shell structure. The ZnPc-COOH loading was down to 0.7 wt% in UCNP@RS with pure-silica shell, although UCNP@RS bears a similar rattle structure.

Upon 980 nm NIR excitation, a remarkable decrease in the red UC luminescence (UCL) emission was observed for UCNP@ROS with ZnPc-COOH loaded (UCNP@ROS-ZnPc-COOH), which verifies the efficient energy transfer from UCNPs to ZnPc-COOH (Figure 3a). The energy transfer efficiency, defined as $(I_0-I_1)/I_0$, where I_0 and I_1 are the integrated intensities of red UCL emission of the material before and after ZnPc-COOH loading,[8] was determined to be 98% for UCNP@ROS. Such a high value has rarely been reported in UCNP-based PDT systems. Consistently, the UCL lifetime of $^4F_{9/2}$ monitored at 654 nm was found to decrease from 0.30 to 0.17 ms (Figure 3a), whereas the UCL lifetime of $^4S_{3/2}$ monitored at 541 nm only decreased slightly from 0.14 to 0.13 ms (Supporting Information, Figure S7 and Table S2). The energy transfer efficiency depends critically on the distance between the donor and acceptor. In the UCNP@ROS-ZnPc-COOH system, the distance between ZnPc-COOH loaded in the shell and UCNP core is 3–10 nm while those loaded in the cavity could directly contact with UCNP, which allowed efficient nonradiative and/or radiative energy transfer processes. For comparison, the energy transfer efficiency for UCNP@OS and UCNP@RS were only 66% and 41% respectively and their UCL lifetimes of $^4F_{9/2}$ were less shortened (Figure 3b,c).

From UV/Vis absorption spectra, a majority of monomers located at 669 nm and a minority of dimers at 611 nm were observed for ZnPc-COOH in DMF (Figure 4a).[9] In aqueous solution, ZnPc-COOH is apt to self-aggregate to form dimers or oligomers, resulting in a remarkable broadening and blue-shift in the absorption.[9] Dimers or oligomers were dominant when ZnPc-COOH was loaded in UCNP@RS while more than half of monomers were maintained in UCNP@ROS-ZnPc-COOH, indicating the inhibition of ZnPc-COOH self-aggregation by organosilica framework owing to hydrophobic interactions and π–π overlapping. The organosilica also provide a strong adsorption on ZnPc-COOH. In a stability test, no apparent ZnPc-COOH leakage was observed for UCNP@ROS-ZnPc-COOH after being stored in PBS for 7 days (Supporting Information, Figure S8).

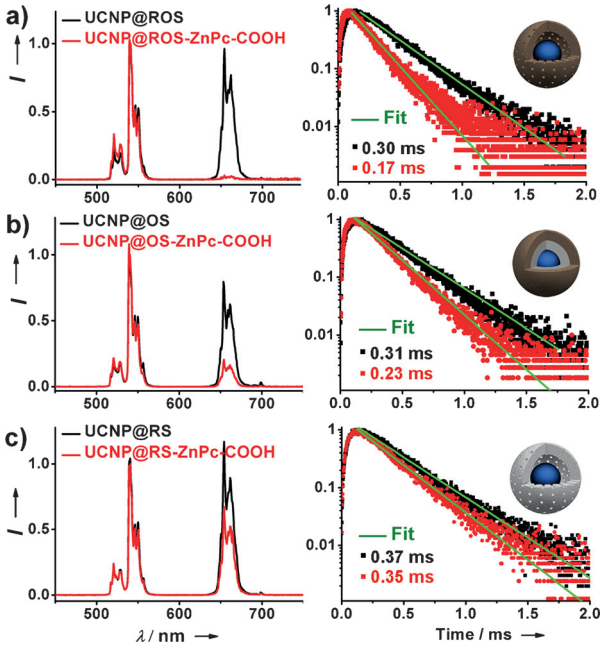

Figure 3. UCL spectra and UCL lifetime of $^4F_{9/2}$ of a) UCNP@ROS, b) UCNP@OS and c) UCNP@RS before and after ZnPc-COOH loading. The lifetime as indicated is determined by fitting the decay with a single exponential function.

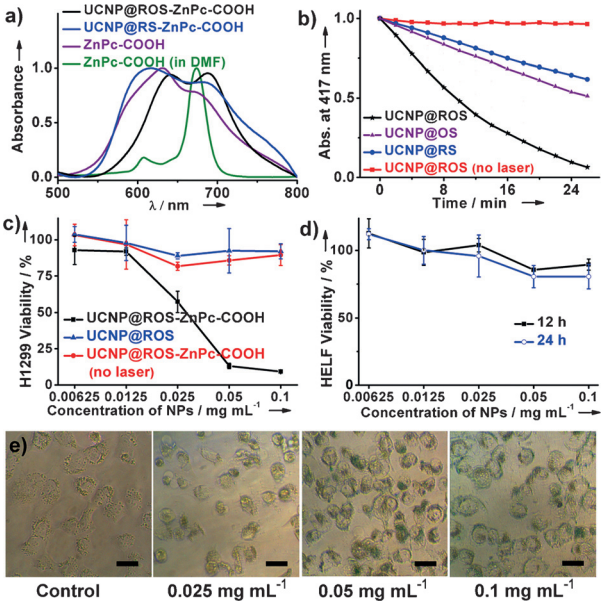

Figure 4. a) UV/Vis spectra of free and loaded ZnPc-COOH dispersed in water (or DMF). b) Curves of time-dependent bleaching of DPBF caused by $^1O_2$ generation in different materials with ZnPc-COOH at 980 nm (ca. 1 Wcm^{-2}). c) Viability of H1299 cells treated with UCNP@ROS-ZnPc-COOH and UCNP@ROS at different concentrations with or without 980 nm irradiation (0.5 Wcm^{-2}). Values are means ± s.e.m. (the experiments for each group were run in duplicate). d) In vitro cytotoxicity of UCNP@ROS-ZnPc-COOH against HELF cells after incubation for 12 h and 24 h. e) Microscopic images of H1299 cells after PDT treatment. (scale bar = 25 μm).

Through energy transfer, ZnPc-COOH can be activated to produce $^1O_2$ with surrounding oxygen molecules. The production of $^1O_2$, which causes direct damage to cancer cells and initiates an inflammatory response, is the key factor for PDT.[10] We then evaluated the ability of UCNP@ROS-ZnPc-COOH to generate $^1O_2$ by measuring the bleaching of 1,3-diphenylisobenzonfuran (DPBF) at 417 nm.[2b] Note that $^1O_2$ was generated by the cooperation of UCNPs and photosensitizers under the NIR irritation. Without NIR irradiation, the DPBF intensity remained essentially unchanged. However, the intensity decreased to below 7% within 26 min at the presence of UCNP@ROS-ZnPc-COOH under 980 nm irradiation (Figure 4b). The rate of bleaching was much more rapid than that of UCNP@OS-ZnPc-COOH or UCNP@RS-ZnPc-COOH under identical conditions, where the intensities decreased to about 50%. As a result of the high loading of ZnPc-COOH, disaggregation effect, and the close proximity between UCNPs and ZnPc-COOH, higher energy transfer efficiency in UCNP@ROS-ZnPc-COOH than that without rattle structure or without organosilica framework was achieved, which thus favored the generation of $^1O_2$.

To assess the in vitro PDT efficacy, we examined the phototoxicity of human lung cancer cells (H1299) after incubation with UCNP@ROS-ZnPc-COOH for 4 h. By means of MTT assay, the H1299 viability was observed to be about 50% with 0.025 mg mL^{-1} of UCNP@ROS-ZnPc-COOH and decreased significantly to about 10% as the concentration higher than 0.05 mg mL^{-1}, upon 980 nm irradiation at a relatively low power density of 0.5 W cm^{-2} for 10 min (Figure 4c). The corresponding microscopic images of H1299 cells clearly showed an increased cell death with the increasing concentration of UCNP@ROS-ZnPc-COOH incubated (Figure 4e), which was consistent with the results of MTT assays. In the control experiments, no significant decline in cell viability was observed for H1299 cells incubated with UCNP@ROS without ZnPc-COOH or UCNP@ROS-ZnPc-COOH without NIR irradiation. The cytotoxicity of UCNP@ROS-ZnPc-COOH was further measured on human embryo lung fibroblasts cells (HELF). After incubation of UCNP@ROS-ZnPc-COOH for 12 and 24 h, the HELF viability was determined to be larger than 80% even at a concentration as high as 0.1 mg mL^{-1} (Figure 4d), implying that UCNP@ROS-ZnPc-COOH was biocompatible and nearly nontoxic to live cells.

Similarly, we found that the proposed PDT platform can be extended to other photosensitizers like rose Bengal (RB). In contrast to ZnPc-COOH, RB is hydrophilic and absorbs the green emission of UCNPs. UCNP@ROS exhibited higher loading capacity and energy transfer efficiency than the UCNP@OS or UCNP@RS platform (Supporting Information, Table S3 and Figure S9). UV/Vis spectra showed that organosilica shell enabled disaggregation of RB (Supporting Information, Figure S10).[11]

Besides PDT application, UCNP@ROS can be used for multimodal imaging of cancer cell by utilizing its intense UCL from the doped Er^{3+} and the high X-ray absorption capability of Lu. After incubation with H1299 cells, strong green and red UC emissions of Er^{3+} were clearly visualized in the cells upon 980 nm irradiation (Figure 5a). Furthermore, as a proof-of-concept experiment, we recorded in vitro color-mapped CT images using an aqueous solution of UCNP@ROS with concentrations of 1.25–10 mg mL^{-1}. As the concentration of UCNP@ROS increased, the CT positive contrast enhancement signals increased in color-mapped CT images (Figure 5b). The CT value of UCNP@ROS, expressed in Hounsfield units (HU), at 10 mg mL^{-1} was 165 HU, which is higher than that of the commercial CT contrast agent, iopromide (140 HU at the same concentration; Figure 5c). Owing to the amine groups on the organosilica shell, we are able to further conjugate cancer-targeting moieties to the surface of UCNP@ROS and enhance its selectivity for cancers. ATF has a high binding affinity to uPAR, which is an important type of tumor marker and over-expressed in H1299 cells.[5a] We conjugated UCNP@ROS with ATF by a facile bioconjugate method.[5b] The cellular uptake experiments demonstrated that the ATF-coupling UCNP@ROS (UCNP@ROS-ATF) can be specifically targeted to H1299 cells, whereas the uptakes of HELF cells were found nearly the same for either UCNP@ROS-ATF or UCNP@ROS NPs (Supporting Information, Figure S11). Importantly, the cancer targeting of UCNP@ROS-ATF was maintained after loading of photosensitizers (Supporting Information, Figure S11). In vivo targeted PDT and imaging through intravenous injection of these nanoprobes deserves further study prior to their further application.

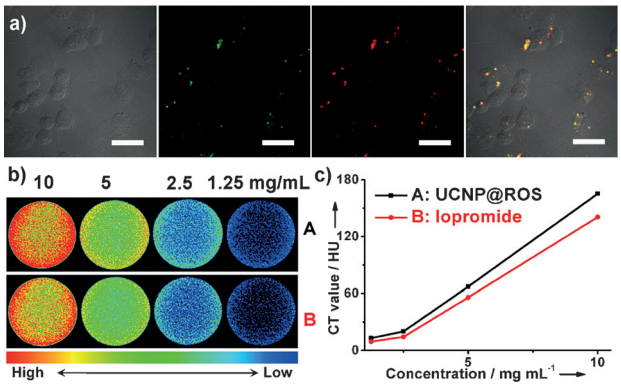

Figure 5. a) Confocal laser scanning microscopy (CLSM) images of H1299 cells after incubation with UCNP@ROS for 4 h at 37 °C. Panels 1–3 show the bright-field image and green and red UCL images, respectively. Panel 4 is the overlay image of panels (scale bar = 40 μm). b) Color-mapped CT images of cross-section of the centrifuge tubes. c) The CT value of UCNP@ROS in aqueous solution at different concentrations.

In summary, we have developed a general strategy to fabricate multifunctional sub-50 nm nano-bioprobes based on a β-$NaLuF_4$:Gd/Yb/Er core and an organosilica shell. Rattle structure and aromatic framework have been smartly designed for loading photosensitizers with high capacity, shortening distance between UCNPs and photosensitizers, and inhibiting the self-aggregation of photosensitizers, all of which are critical for improving PDT efficacy. In particular, ZnPc-COOH was loaded in the rattle-structured nanoprobes with a capacity up to 7.7 wt% and an UC energy transfer efficiency as high as 98% was thus achieved. The high NIR-triggered PDT efficacy against cancer cells and biological

safety were demonstrated in vitro. Combined with the additional functions including UC/CT bimodal imaging and tumor-targeting, these nano-bioprobes will be highly promising for the development of multiplex theranostic nanoplatforms.

Keywords: multimodal imaging · organosilica · photodynamic therapy · rattle structures · upconversion nanoprobes

How to cite: *Angew. Chem. Int. Ed.* **2015**, *54*, 7915–7919
Angew. Chem. **2015**, *127*, 8026–8030

[1] a) F. Wang, D. Banerjee, Y. S. Liu, X. Y. Chen, X. G. Liu, *Analyst* **2010**, *135*, 1839; b) G. F. Wang, Q. Peng, Y. D. Li, *Acc. Chem. Res.* **2011**, *44*, 322; c) M. L. Deng, L. Y. Wang, *Nano Res.* **2014**, *7*, 782.

[2] a) N. M. Idris, M. K. Gnanasammandhan, J. Zhang, P. C. Ho, R. Mahendran, Y. Zhang, *Nat. Med.* **2012**, *18*, 1580; b) M. Wang, Z. Chen, W. Zheng, H. M. Zhu, S. Lu, E. Ma, D. T. Tu, S. Y. Zhou, M. D. Huang, X. Y. Chen, *Nanoscale* **2014**, *6*, 8274.

[3] a) P. Zhang, W. Steelant, M. Kumar, M. Scholfield, *J. Am. Chem. Soc.* **2007**, *129*, 4526; b) H. S. Qian, H. C. Guo, P. C. L. Ho, R. Mahendran, Y. Zhang, *Small* **2009**, *5*, 2285; c) X. F. Qiao, J. C. Zhou, J. W. Xiao, Y. F. Wang, L. D. Sun, C. H. Yan, *Nanoscale* **2012**, *4*, 4611.

[4] a) Q. Zhang, J. P. Ge, J. Goebl, Y. X. Hu, Z. D. Lu, Y. D. Yin, *Nano Res.* **2009**, *2*, 583; b) X. J. Kang, Z. Y. Cheng, D. M. Yang, P. A. Ma, M. M. Shang, C. Peng, Y. L. Dai, J. Lin, *Adv. Funct. Mater.* **2012**, *22*, 1470; c) W. P. Fan, B. Shen, W. B. Bu, F. Chen, K. L. Zhao, S. J. Zhang, L. P. Zhou, W. J. Peng, Q. F. Xiao, H. Y. Xing, J. N. Liu, D. L. Ni, Q. J. He, J. L. Shi, *J. Am. Chem. Soc.* **2013**, *135*, 6494; d) L. Z. Zhao, J. J. Peng, Q. Huang, C. Y. Li, M. Chen, Y. Sun, Q. N. Lin, L. Y. Zhu, F. Y. Li, *Adv. Funct. Mater.* **2014**, *24*, 363; e) W. P. Fan, B. Shen, W. B. Bu, F. Chen, Q. J. He, K. L. Zhao, S. J. Zhang, L. P. Zhou, W. J. Peng, Q. F. Xiao, D. L. Ni, J. N. Liu, J. L. Shi, *Biomaterials* **2014**, *35*, 8992; f) J. N. Liu, J. W. Bu, W. B. Bu, S. J. Zhang, L. M. Pan, W. P. Fan, F. Chen, L. P. Zhou, W. J. Peng, K. L. Zhao, J. L. Du, J. L. Shi, *Angew. Chem. Int. Ed.* **2014**, *53*, 4551; *Angew. Chem.* **2014**, *126*, 4639; g) W. P. Fan, B. Shen, W. B. Bu, X. P. Zheng, Q. J. He, Z. W. Cui, K. L. Zhao, S. J. Zhang, J. L. Shi, *Chem. Sci.* **2015**, *6*, 1747.

[5] a) Q. Huai, A. P. Mazar, A. Kuo, G. C. Parry, D. E. Shaw, J. Callahan, Y. D. Li, C. Yuan, C. B. Bian, L. Q. Chen, B. Furie, B. C. Furie, D. B. Cines, M. D. Huang, *Science* **2006**, *311*, 656; b) P. Huang, W. Zheng, S. Y. Zhou, D. T. Tu, Z. Chen, H. M. Zhu, R. F. Li, E. Ma, M. D. Huang, X. Y. Chen, *Angew. Chem. Int. Ed.* **2014**, *53*, 1252; *Angew. Chem.* **2014**, *126*, 1276.

[6] a) Q. Liu, Y. Sun, T. S. Yang, W. Feng, C. G. Li, F. Y. Li, *J. Am. Chem. Soc.* **2011**, *133*, 17122; b) N. J. J. Johnson, F. C. J. M. van Veggel, *Nano Res.* **2013**, *6*, 547.

[7] S. Inagaki, S. Guan, T. Ohsuna, O. Terasaki, *Nature* **2002**, *416*, 304.

[8] Y. Wang, K. Liu, X. M. Liu, K. Dohnalova, T. Gregorkiewicz, X. G. Kong, M. C. G. Aalders, W. J. Buma, H. Zhang, *J. Phys. Chem. Lett.* **2011**, *2*, 2083.

[9] S. Subbiah, R. Mokaya, *J. Phys. Chem. B* **2005**, *109*, 5079.

[10] A. D. Garg, D. Nowis, J. Golab, P. Agostinis, *Apoptosis* **2010**, *15*, 1050.

[11] E. Gianotti, B. M. Estevao, F. Cucinotta, N. Hioka, M. Rizzi, F. Reno, L. Marchese, *Chem. Eur. J.* **2014**, *20*, 10921.

Received: February 14, 2015
Published online: May 26, 2015